Cabled ocean observatory data reveal food supply mechanisms to a cold-water coral reef

Tom Van Engeland[a*+], Olav Rune Godø[b], Espen Johnsen[b], Gerard C. A. Duineveld[c], Dick van Oevelen[a]

[a] NIOZ Royal Netherlands Institute for Sea Research, Department of Estuarine and Delta Systems, and Utrecht University, Korringaweg 7, 4401NT Yerseke, The Netherlands

[b] Institute of Marine Research, PO Box 1870, 5817 Bergen, Norway

[c] NIOZ Royal Netherlands Institute for Sea Research, Department of Ocean Systems, and Utrecht University, Landsdiep 4, 1797 SZ 't Horntje (Texel), The Netherlands

Author emails:

Tom Van Engeland: Tom.Van.Engeland@gmail.com

Olav Rune Godø: Olav.Rune.Godoe@imr.no

Espen Johnsen: Espen.Johnsen@imr.no

Gerard Duineveld: Gerard.Duineveld@nioz.nl

Dick van Oevelen: Dick.van.Oevelen@nioz.nl

keywords: cold-water corals / hydrodynamics / acoustic backscatter / continuous monitoring / ocean observatory / Norway

* Corresponding author, Tom.VanEngeland@uantwerpen.be

[+] Present address: University of Antwerp, Department of Biology, Campus Drie Eiken Universiteitsplein 1, room D.C.126,2610 Wilrijk , Belgium; Tel: +32 474 59 15 37

Abstract

We investigated food supply mechanisms to a cold-water coral (CWC) reef at 260 m depth on the Norwegian continental shelf using data from a cabled ocean observatory equipped with Acoustic Doppler Current Profilers (ADCPs), an echosounder, and sensors for chlorophyll, turbidity and hydrography in the benthic boundary layer (BBL). Tidal currents of up to tens of cm s^{-1} dominated BBL hydrodynamics while residual currents were weak (~10 cm s^{-1}), emphasizing a supply and high retention of locally produced phytodetritus within the trough. A direct connection between the reefs and surface organic matter (OM) was established by turbulent mixing and passive particle settling, but relative contributions varied seasonally. Fresh OM from a spring-bloom was quickly mixed into the BBL, but temperature stratification in summer reduced the surface-to-bottom connectivity and reduced the phytodetritus supply. A qualitative comparison among acoustic backscatter in the ADCPs (600 kHz, 190 kHz) and echosounder (70 kHz) suggests that vertically migrating zooplankton may present an alternative food source in summer. Nocturnal feeding by zooplankton in the upper water column sustains downward OM transport independent from water column mixing and may dominate as food supply pathway over sedimentation of the phytodetritus, especially during stratified conditions. In addition, it could present a concentrating mechanism for nutritional components as compensation for the deteriorating phytodetritus quality. Overall, the observed patterns suggest seasonal changes in the food supply pathways to the reef communities. The moderating role of temperature stratification in phytodetritus transport suggests stronger dependence of the cold-water corals on zooplankton for their dietary requirements with increased stratification under future climate scenarios. This study demonstrates the added value of permanent ocean observatories to research based on dedicated campaigns and regular monitoring.

1. Introduction

Cold-water coral (CWC) reef communities are metabolic hotspots on the seafloor (Van Oevelen et al. 2009; White et al. 2012; Cathalot et al. 2015; Rovelli et al. 2015) with organic matter processing rates that are up to 20 times higher than those of the surrounding soft sediments. Such high processing rates require a sufficient supply of organic matter to these reef systems. CWCs and the associated biota may utilise a range of food sources, including dissolved organic matter, phytodetritus, suspended bacteria and zooplankton (Kiriakoulakis et al. 2005; Duineveld et al. 2007; Dodds et al. 2009; Purser et al. 2010; Mueller et al. 2014). Opportunistic feeding is a strategy that enables them to meet their energetic and nutritional requirements in a broad range of conditions, including bloom and non-bloom periods (Khripounoff et al. 2014; Mueller et al. 2014), but the mechanisms that transport these potential resources to the reefs are difficult to untangle.

Various particulate and dissolved organic matter (POM and DOM) sources are produced in the sunlit surface ocean. Whereas DOM needs to be transported to potential consumers (e.g. sponges and cold-water corals; de Goeij et al. 2013, Gori et al. 2014, Mueller et al. 2014) by water movement, which may be advective or turbulent, POM can arrive at the seafloor through gravitational sinking. However, passive organic particle sinking is generally considered insufficient to meet the high metabolic demands of reef communities in the North-Atlantic (Soetaert et al. 2016). An advective environment is therefore essential for the food supply CWC reefs (Thiem et al. 2006; Mienis et al. 2007; Duineveld et al. 2007; Davies et al. 2009; Soetaert et al. 2016). CWCs are found on topographic features that are naturally exposed to enhanced current velocities, including sills (Lavaleye et al. 2009; Wagner et al. 2011), canyon walls (Huvenne et al. 2011; Khripounoff et al. 2014) and the continental shelf break (Thiem et al. 2006). Enhanced currents may also resuspend previously settled POM, that is subsequently transported to the reefs (Carlier et al. 2009). CWCs do not only inhabit topographic

features on the seafloor, but also modify the seafloor topography through the formation of biogenic reefs and mounds (Roberts 2006) that protrude tens (Correa et al. 2012; Cathalot et al. 2015) to hundreds (De Mol et al. 2002; Van Weering et al. 2003) of meters above the seafloor. These biogenic topographies interact with stratified flows causing internal waves and turbulence with pronounced vertical current components (Mohn et al. 2014; Cyr et al. 2016). Under a tidal regime, this interaction may result in episodic downwelling of organic matter pulses from the surface to the CWC reef communities (Davies et al. 2009; Findlay et al. 2013; Soetaert et al. 2016).

Feeding experiments, stable isotopes, fatty acid analysis and video observations suggest that zooplankton can present another important food source to CWC (e.g. Duineveld et al. 2007; Dodds et al. 2010; Purser et al. 2010; Naumann et al. 2011; Gori et al. 2015; Van Oevelen et al. 2018). However, it remains challenging to assess the importance of zooplankton as organic matter source for CWCs. Some zooplankton taxa migrate vertically to feed on surface phytoplankton during the night and find shelter from predators in the deeper water at daytime (Hays 2003). In the Gulf of Mexico diel migration of nekton down to two CWC reef systems has been observed with continuous acoustic doppler current profiler (ADCP) measurements (Mienis et al. 2012), suggesting that part of the migrating community may form an additional food source to the CWC communities (Hebbeln et al. 2014). The vertical migration capacity of zooplankton, such as copepods and euphausiids, implies that their presence at CWC reefs is less dependent on advection than that of other organic matter sources.

It is evident that CWC reef communities can be supported by a range of potential food sources for which transport mechanisms are controlled by various physical and biological factors on scales of hours to weeks. Seasonal variation in for example phytoplankton concentration (Duineveld et al. 2007), water-column stratification and wind forcing are superimposed on this short-term variability (Thiem et

al. 2006). Identifying food supply pathways therefore requires a long-term multi-dimensional observational approach, in addition to dedicated short-term campaigns. Several integrative studies have been conducted, but these usually cover weeks of observation (e.g. Duineveld et al. 2012; Hebbeln et al. 2014) and focus on near-bed processes (Mienis et al. 2007; Khripounoff et al. 2014). Ocean observatories provide a means to combine long-term measurement efforts with the required high temporal resolution (Roberts et al. 2005; Soltwedel et al. 2005) to elucidate oceanic processes and present a valuable addition to routine monitoring for both management and scientific purposes (Godø et al. 2014).

The Norwegian continental shelf hosts among the highest abundance of CWC reefs in the world (Roberts et al. 2006). To better understand their biological and physical settings, a cabled observatory has been installed in the Hola trough, an area with CWC mounds off the Norwegian coast (Godø et al. 2012b, 2014; Fig. 1). We used data from this observatory to resolve the seasonality of the physical and biological settings that govern food supply to a CWC reef. More specifically we used observatory data from the years 2014 and 2015 on current velocities throughout the water column, hydrographic parameters, and several proxies for subclasses of POM to (1) assess food availability throughout a productive season by characterising the variability in different food sources, and (2) identify the most important transport mechanisms that bring these food sources to the CWC reef communities.

2. Materials and methods

2.1 Location of the LoVe observatory

The LoVe (Lofoten-Vesterålen) ocean observatory is located 20 km from the Lofoten Islands (Norway) in the Hola trough (Fig. 1). This glacially-deepened trough of 180 – 260 m deep incises the continental shelf in a north-west to south-east direction from the continental slope to the coast. The location of the

observatory (~260 m deep) is enclosed by the two 100-m deep banks; Vesterålsgrunnen in the northeast and Eggagrunnen in the southwest. The trough has a diverse topography with sand wave fields of up to 7 m high, 10 to 35 m high ridges and approximately 20 m high CWC mounds (Bøe et al. 2009). The CWC mounds are predominantly found in the south-eastern part of the trough at a depth of ~260 m just south of the Vesterålsgrunnen bank.

No detailed analysis has been performed on the community composition or the reef mounds in the Hola trough, but still images show that the dominant reef-building coral species is *Lophelia pertusa* (Osterloff et al. 2016b). This scleractinian coral is the dominant reef builder in European waters (Roberts et al. 2006), although *Madrepora oculata* can also occur as smaller parts of the reefs on the Norwegian shelf (Järnegren and Kutti 2014). Still images also show a high abundance of shrimps, presence of the redbass *Sebastes* sp. and soft-coral specimens including *Paragorgia arborea (Osterloff et al. 2016b, http://love.statoil.com),* which are typical members of Norwegian reefs (Fosså et al. 2002) Other filter-feeding community members that are usually associated with the *Lophelia* framework are the soft coral, *Primnoa resedaeformis*, sponges (e.g. *Mycale lingua*) and bivalves (e.g. *Acesta excavata;* Järnegren and Kutti 2014, De Clippele et al. 2015*).*

The coral mounds are associated with trailing erosional scour marks that hint at a local predominant northward or north-westward current direction. These scour mark patterns are consistent with an anti-clockwise circulation, which is characteristic for these northern troughs (Buhl-Mortensen et al. 2012). However, local lithology also suggests a high spatial variability in current direction and strength, ranging from several cm s^{-1} to 1 m s^{-1} (Bøe et al. 2009). The seafloor in the coral-dominated part of the through slopes at an angle of approximately 4º in a north-east direction towards the Vesterålsgrunnen bank (Godø et al. 2012b).

The spatial-temporal variability in current structures and water transport is further influenced by two major current systems. Firstly, the North Atlantic Current (NAC) transports comparatively warm saline

North Atlantic Water (NAW) northward along the continental shelf edge. This water mass is usually identified by salinities in excess of 35 (Pedersen et al. 2005, Zhu et al. 2009, Skagseth et al. 2011). Secondly, the Norwegian Coastal Current (NCC) transports cold, less saline, Norwegian Coastal Water (NCW) northward along the coast, with current velocities in excess of 1 m s^{-1} (Ersdal 2001). This water mass is characterised by salinities below ~34.5 (Pedersen et al. 2005, Zhu et al. 2009, Skagseth et al. 2011) In general, NCW has a stronger influence on the shallower banks, while the NAW is more restricted to the deeper troughs such as the Hola trough. However, this pattern varies seasonally. During winter the NCW forms a deeper wedge close to the coast, while in summer it exists as wider thinner layer that covers the larger part of the continental shelf (Skagseth et al. 2011, and references therein). The inflow of NAW in the northern glacial troughs varies over time and depends on, among others, the interplay between the strength of the NAC and trough morphology (Sundby 1984). Because of gradual mixing of NAW and NCW in northward direction, salinity signatures show less contrast in the northern troughs (Pedersen et al. 2005). Mixing of both water masses is facilitated in winter and spring by mesoscale eddies that find their origin in the topographic steering of the NCC, that takes the form of a coastal jet at this time (Buhl-Mortensen et al. 2012) .

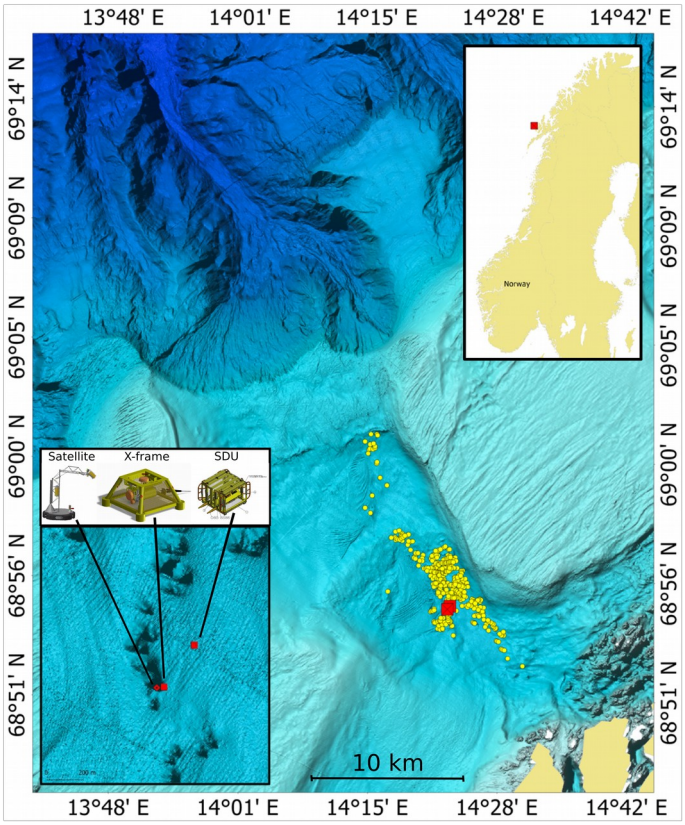

Fig. 1: Overview of the observatory's location (red squares) in the Hola trough. The relevant region is scattered with coral mounds (yellow dots). The sensor platforms (satellite and X-frame) are located near a cold-water coral mound (lower left).

2.2 Infrastructure of the LoVe observatory

The LoVe observatory was launched in September 2013 and has a modular configuration consisting of three connected subunits (Fig. 1): (1) the Subsea Distribution Unit (SDU), (2) the X-frame and (3) the satellite unit. The SDU is connected with a cable to the main land for power supply and data transfer. The X-frame is connected to the SDU and contains, amongst others, an upward-looking 3-beam 600 kHz Nortek Aquadopp Acoustic Doppler Current Profiler (ADCP, henceforth called short-range or SR-ADCP), an upward-looking 3-beam 190 kHz Nortek Continental ADCP (henceforth called long-range or LR-ADCP) and an upward-looking 70 kHz Simrad EK60 echosounder. The satellite unit is placed within meters of the CWC reef framework and has a still camera, hydrophone and sensors for salinity,

temperature, chlorophyll *a*, turbidity, and pressure (depth). Technical details of the three subunits and sensors are available on the website dedicated to the observatory (http://love.statoil.com). This website is also a portal to all data and still images, which are publicly available. The data used in this manuscript were downloaded from the website on December 9, 2015.

2.3 Data selection

2.3.1 LoVe observatory data

This study focused on variables that were measured in 2015 relating to water movement, particle concentration, and hydrography, because this is the most complete data set of the two years (2014-2015) ensuring the best overlap between the ADCPs and other sensors. The SR-ADCP measured from 0.5 to 40.5 mab (meters above bottom) with a bin size of 2 m. The LR-ADCP measured from 2 mab to the surface (262 mab) with a bin size of 5 m. Both systems measured current velocities in a geographic reference system (East–North–Up) in 10-minute intervals. Hourly sampled data on chlorophyll a fluorescence (Seapoint), turbidity (Seapoint), salinity, pressure (used as proxy for tides), and temperature were available from multi-sensor probes on the satellite unit. But part of these time series was not available due to sensor malfunction (see below and appendix).

Echosounder data were compared with the ADCP backscatter intensities. Whereas ADCPs are developed to measure velocities and produce acoustic backscatter information as by-product, echosounders are designed to monitor acoustic backscatter, mainly from fish and zooplankton. The echosounder operates at 70 kHz with a ping rate of 2 s^{-1}. The system was calibrated using the standard sphere method (Foote et al. 1987) before launch, but no calibration at depth was available to compensate for potential changes of instrument performance with time and/or depth. Acoustic data were processed and visualized using the LSSS software package (Korneliussen et al. 2016). One echosounder time series from before and one from after the spring bloom were included in this study to

contrast against the uncalibrated ADCP backscatter intensities.

2.3.1 Complementary and climate data

Chlorophyll a concentration and sea surface temperature (SST) data from the MODIS-Aqua satellite platform were downloaded for the year 2015 as additional external data (OBPG, 2017) in order to (1) check for data consistency, and (2) place the local observations at LoVe observatory in a larger spatial context. The 8-day standard mapped image composites with a spatial resolution of 4 km were used to obtain a consistent coverage for a maximal time span (no winter values due to solar zenith-related limitation of the atmospheric correction algorithms) and to reduce the impact of local cloud cover. In these level-3 products, chlorophyll a is estimated with the OCx algorithm merged with a colour index (https://oceancolor.gsfc.nasa.gov/atbd/chlor_a/, and references therein), and SST is derived from the 11-12 µm long-wave radiation in the underlying satellite data (https://oceancolor.gsfc.nasa.gov/atbd/sst/, and references therein).

Wind speed and direction data for the period 2014 – 2015 from the weather station at Bø, Vesterålen, were downloaded from the "eKlima" data portal (eklima.met.no) from the Norwegian meteorological institute.

2.4 Data download and processing

2.4.1 ADCP

ADCP data were downloaded from the data portal of the observatory as raw binary output files from the respective devices. Conversions from binary to ASCII were performed with the Continental and Aquapro software packages from Nortek AS. Individual ASCII files, containing data for a few days at 10-minute intervals, were imported into R Statistical Software (R Core Team 2016). Velocity data were taken at 10-minute sampling intervals and consecutive data files usually had temporal gaps of not more

than 30 minutes between them. To obtain regular samples, time series data were binned per hour by taking median values. Remaining gaps were filled in by linear interpolation if longer regularly sampled time series were needed for particular analyses. Care was taken not to interpret potential artefacts that might arise from this interpolation (see for instance section 3.1).

Velocity readings from the ADCPs that were associated with raw backscatter data below the theoretical thresholds (45 and 33 counts for the Continental and Aquadopp respectively; Nortek forum) were replaced by linearly interpolated values (along the time dimension). The velocity readings above 120 mab from the LR-ADCP had to be discarded because of a systematic bias, most likely due to low backscatter intensities or high noise levels in one of the beams (Appendix). The SR-ADCP velocity data above 20 mab were also associated with large uncertainty (Appendix). Because of the larger range of the LR-ADCP, the limited added value of the higher resolution in the SR-ADCP, and its velocity discrepancies with the LR-ADCP between 20 and 40 mab (see section 3. and Appendix), only the current velocities from the LR-ADCP are reported here. The acoustic backscatter intensity was investigated over the entire profiles (20 and 46 cells in the SR-ADCP and LR-ADCP respectively). Backscatter intensities were corrected for beam spreading, including non-spherical spreading in the near field (Downing 1995), and sound attenuation along the beams due to the water.

2.4.2 Echosounder

The echosounder data were downloaded and examined with LSSS software package. Thresholding of s_V (acoustic volume backscattering coefficient) was used to study vertical distribution patterns and dynamics of organisms of various sizes. This approach facilitated an appropriate comparison of the echosounder and ADCP backscattering data.

2.4.3 Other LoVe variables

Turbidity, salinity, temperature, depth, and chlorophyll a and coloured DOM data were downloaded as single ASCII text files per variable with hourly values. Environmental variables were checked for sensor saturation and noise levels. Based on these checks, we decided to use only the chlorophyll a fluorescence data (raw values) and the hydrographic parameters and discard the turbidity and coloured DOM data (Appendix).

2.4.4 Satellite and climate/weather data

From the chlorophyll a imagery that was downloaded from the NASA Ocean Color website (https://oceancolor.gsfc.nasa.gov; cf. section 2.3.1) on in February 2017, two subsets were selected: (1) a local subset covering a square of 10 by 10 nautical miles centred around the X-frame location (henceforth referred to as local chlorophyll signal), and (2) a regional subset covering the larger part of the Hola trough (bounding box: 67º 36' N, 8º E – 69º 24'N, 16º 54' E; henceforth referred to as regional chlorophyll signal). From the SST imagery that was downloaded together with the chlorophyll imagery, only the local subset was selected and used to estimate a seasonal trend by spline smoothing. 95% estimation bands were constructed from jacknife residuals of this smooth spline estimation.

2.5 Data analysis

2.5.1 Time series analysis techniques

Spectral analyses were used to identify the scales that contributed significantly to the overall variance in the various time series, and coherence analysis was used to study the co-variation between different time series (e.g. Shumway and Stoffer 2006).

Coherence and spectral analyses are based on either a Fourier transformation (standard frequency domain analysis; e.g. Bloomfield 2000) or a wavelet transformation (e.g. Percival and Walden 2000). Here we used both transformations to analyse the same process or relationship. If the wavelet-based

analysis gave the same result as Fourier-based analysis, the Fourier-based method was reported because of the higher frequency resolution. If results of both approaches differed because of a limited temporal extent of the investigated process/relationship, only the results from the wavelet-based method were reported. As a result, variance contributions from tidal drivers are here reported with Fourier-based methods (see section 3.2), while wavelet-based results are reported the mixing regimes. Wavelet-based coherence was calculated using a continuous wavelet transform with a complex Morlet wavelet (Torrence and Compo 1998).

Smoothing and frequency band selection from time series were accomplished, where applicable, by multi-resolution decompositions, based on the Maximal Overlap Discrete Wavelet Transform (MODWT with symlet s8 as filter; Daubechies 1992, Mallat 1999). In contrast to the observatory data, the Modis-Aqua SST data were smoothed with smooth spline estimation, because the occurrence of multiple values per time point (due to spatial extent of the selected region) excluded wavelet-based smoothing.

2.5.2 Acoustic backscatter (ADCP)

Linear relationships between acoustic backscatter and suspended matter proxies (chlorophyll a, bottom current speed as proxy for resuspended material) were investigated by means of linear regression analysis (Gostiaux and Van Haren 2010). Logarithmic transformations were applied whenever needed to obtain symmetric residual distributions.

All data manipulation and analyses were performed in R Statistical Software (R Core Team 2016). Wavelet analyses were performed with the R-packages 'waveslim' (Whitcher 2015) and 'wmtsa' (Constantine and Percival 2013) for the discrete methods, and ‘biwavelet’ for the continuous wavelet methods (Gouhier et al. 2016).

3. Results

3.1 Hydrography

Bottom water temperature (BWT) varied between 8 and 9 ºC in the period November 2014 to February 2015, after which it decreased to values between 6.5 and 8 ºC (Fig. 2A). From the second half of May onwards BWT values gradually increased again to winter values above 8 ºC. Bottom water salinity (BWS) exhibited a fairly weak seasonal signal with values ranging between 34.3 and 35.0 in the period November 2014 - April 2015, followed by a sudden decrease at the end of April to 33.8 and a gradual increase to > 34.5 throughout the remainder of 2015. Whether this is a yearly recurring pattern is not clear from the observatory data (Appendix).

A comparison of the 2015 BWT signal with an average sea surface temperature (SST) signal from the MODIS-Aqua satellite revealed three distinct hydrographic periods (Fig. 2A): (1) during early winter (November to January) SST was similar to BWT, (2) from January to May, the SST fell below the BWT, and (3) from June until the end of October, the SST was higher than the BWT.
Wavelet coherence analysis of the BWT and BWS revealed strong coherence in spring (Fig. 2B), indicating strong covariation between these signals. This was also reflected in a positive correlation between BWT and BWS changes (Fig. 2A; middle inset). The period of high coherence between BWT and BWS coincided with high wind speeds (Fig. 3A). When SST increased above the bottom water temperature, coherence weakened (Fig. 2A; right inset). CTD data from a maintenance cruise from June 2015 indicated that during this period of low coherence between BWT and BWS, temperature stratification had developed (Fig. 3B). Note that figure 2B shows two artefacts from linear interpolation at the beginning of March and at the end of May, respectively. Since these reside mainly in the lower scales and are localized in time, they do not affect the overall outcome of this analysis.

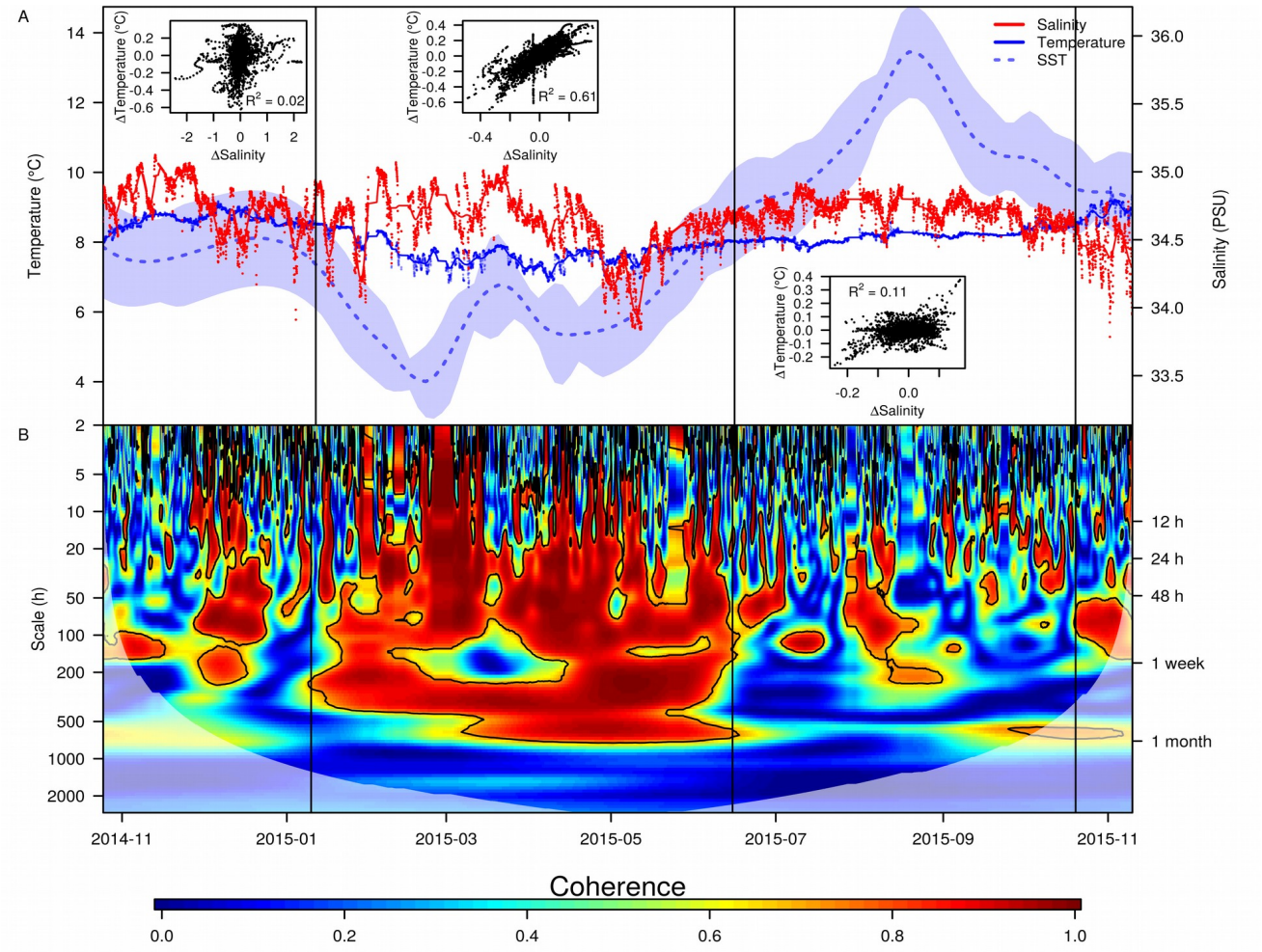

Fig. 2: Time series plots (A) of sea surface temperature (SST; blue dashed), bottom water temperature (BWT; blue solid), and bottom water salinity (BWS; solid red), and wavelet coherence analysis of the BWT and BWS series (B). The blue envelope around the SST signal (spline) is the approximate 95% estimation interval based on jacknife residuals. Raw BWT and BWS values are given as points; the corresponding lines are the smooth signals of a Maximal Overlap Discrete Wavelet Transform (MODWT)-based multiresolution decomposition, that exclude tidal variability. The small scatterplots in panel A depict the linear relationships between the first differences (Δ) of BWS and BWT for the regimes indicated by the vertical lines.

344

A

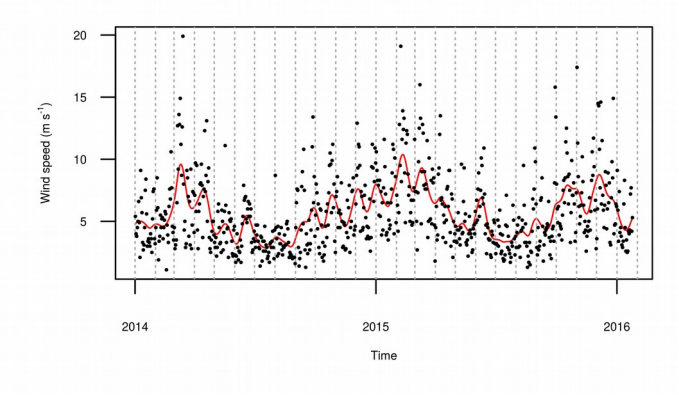

B.

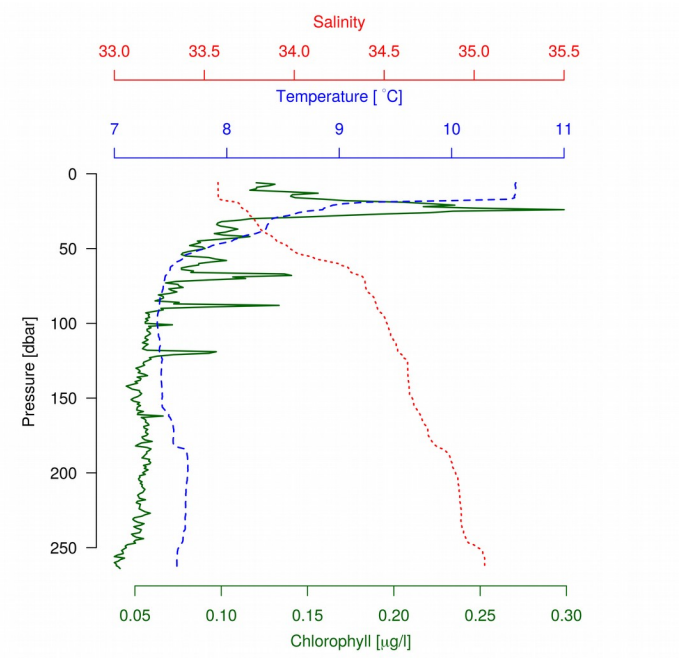

345 Fig. 3: Panel A: Wind speed data near Bø from eKlima (black dots) with a smoothed trend line (red).
346 Winter and spring are characterised by high wind speeds. Panel B: Vertical profile of salinity (red
347 dotted line), temperature (blue dashed line) and chlorophyll a concentration (green solid line) near the
348 observatory during a maintenance cruise from June 2015. The summer chlorophyll maximum resides in
349 the upper mixed layer of the water column.

3.2 Hydrodynamics

The highest current speeds in the lower 120 m of the water column were 1 m s^{-1} (99.9-percentile of the hourly median values), but 90% of the values were below 0.34 m s^{-1}. In the lower 20 meters the velocity distribution was very similar, with 0.89 m s^{-1} and 0.34 as 99.9- and 90-percentile, respectively. In general, current velocities exhibited similar variation at different depths throughout the water measured column (data not shown). From January to May and in November, events with strong V_{east} and (to a lesser extent) V_{north} components were observed (data not shown), which covered the water column from 0 to 120 mab and often coincided with increased wind stress. But a clear 1:1 relationship with wind speeds was not found (data not shown).

Two dominant current directions were observed at 10 mab (Fig. 4A). The vertical velocity component of the LR-ADCP exhibited an upward bias of approximately 2.5 cm s^{-1}, relative to the SR-ADCP measurements (i.e. the distribution of the SR-ADCP vertical velocities at 10 mab was similar to that of the LR-ADCP (Fig. 4C), except that the point cloud was centered on the horizontal axis rather than above it; Appendix). The origin of this bias is currently unknown. Taking this bias into account, south-to south-westward currents were directed downward, whereas north-eastward currents had a positive vertical velocity component due to topographic steering (Fig. 4C; remember the overall upward bias). Higher current velocities in excess of 0.5 m s^{-1} were fairly specific south-to-south-westward, or varied from north to southeast (Fig. 4C). In contrast, at 100 mab low and moderate current velocities (< 0.4 m s^{-1}) were less specific in direction, but higher velocities tended to cluster along a north-east and east direction (Fig. 4B). No clear relationship between the vertical and horizontal components existed at 100 mab (Fig. 4D). Westward currents were rare at both 10 and 100 mab.

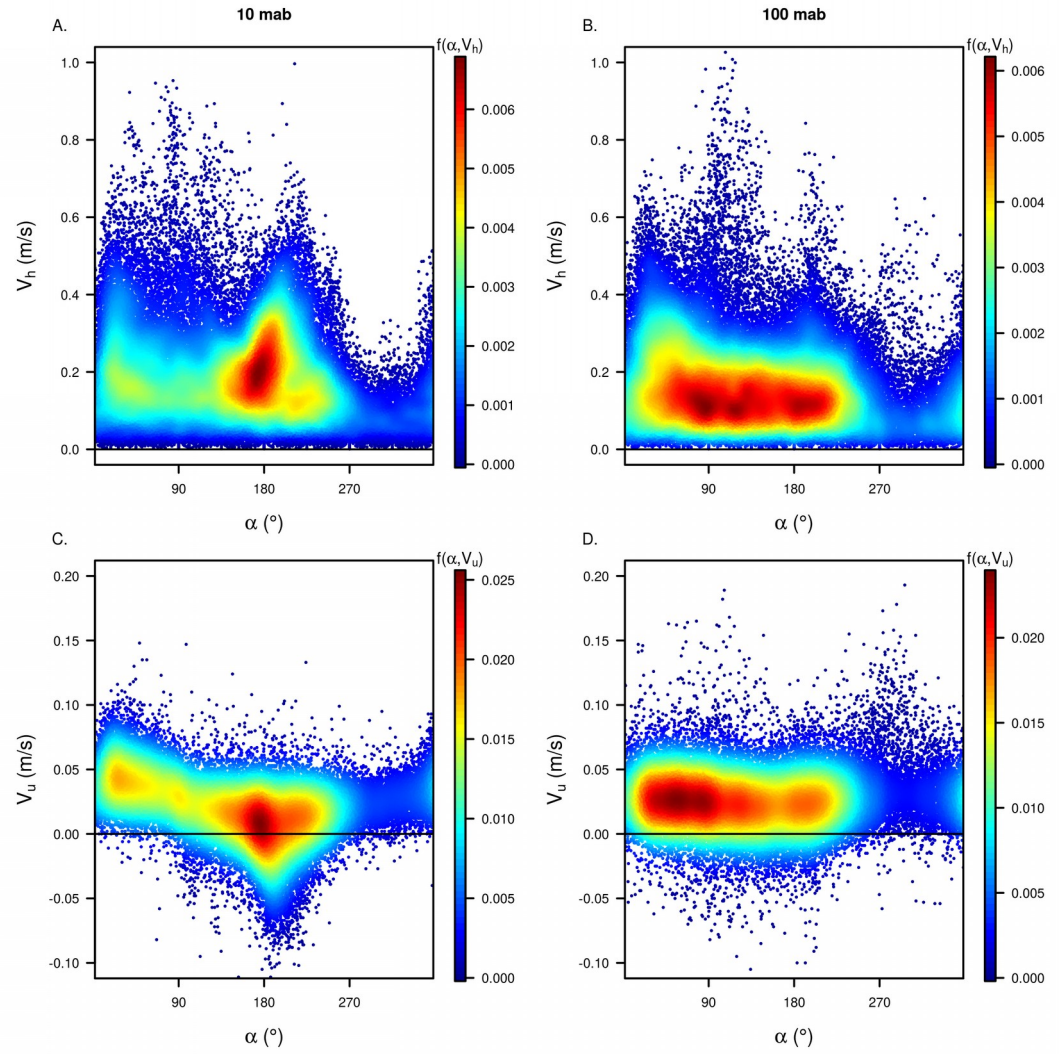

Fig. 4: Horizontal (V_h, panels A and B) and vertical (V_u, panels C and D) current velocity components as function of current heading at 10 meters above the bottom (panels A and C) and 100 meters above the bottom (panels B and D). Colors represent the density function (f(α,V.) estimated via 2D kernel smoothing.

The variance-preserving spectrum of water height (i.e. pressure) showed a high contribution of a semi-diurnal and a lower contribution of a diurnal tidal periodicity, indicating that the tidal height is dominated by a semi-diurnal periodicity (Fig. 5A). In contrast, the horizontal velocity components from 100 mab showed a predominant diurnal contribution in their overall variance spectrum. This resulted in a clear coherence between the tidal signal (water depth) and V_{north} at both frequencies (the semi-diurnal and diurnal frequency), while coherence of V_{east} at the semidiurnal scale was low. Elevated coherence

values were also found at frequencies related to the spring-neap tidal cycle (i.e. 6 and 13 days), but their contribution in the respective spectra (i.e. overall variance) was low. No dominant frequencies were identified in the vertical velocity component at 100 mab. At 10 mab, horizontal velocity components showed similar variability and coherence to tides as at 100 mab (data not shown). The vertical current velocity component at 10 mab exhibited significant diurnal variation, similar to the horizontal components. This variability is visible as the upward and downward tails in figure 4C.

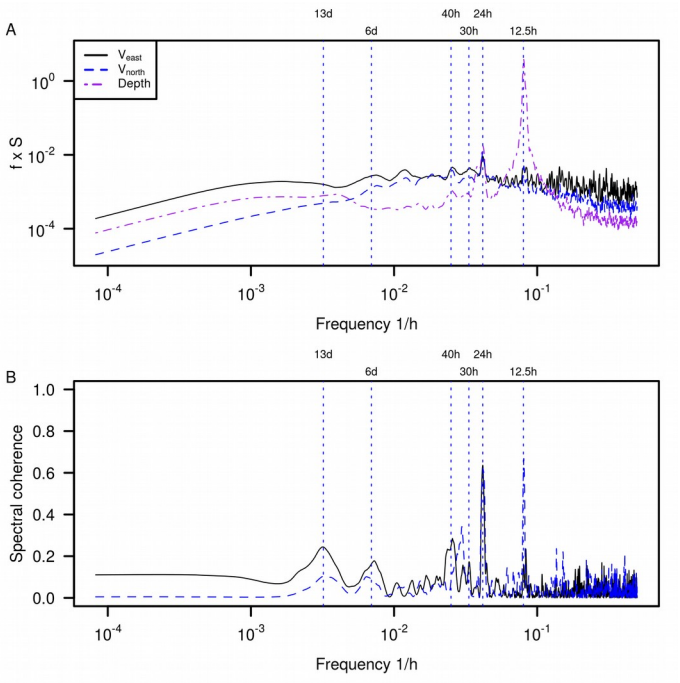

Fig. 5: Variance preserving spectrum (f x S = frequency x spectrum; panel A) of the horizontal current velocity components (V_{east} = black solid line, and V_{north} = blue dashed line) and their spectral coherence (panel B) with the tidal signal (water depth = purple line in spectral plot). Periodicities that are associated with tides or relevant in this analysis are indicated at the top of the graphs.

The residual east and north velocity components at 10 mab averaged 3 ± 7 cm s^{-1} and -5 ± 5 cm s^{-1}, respectively and the residual east and north components at 100 mab averaged at 4 ± 11 cm s^{-1} and -0.6 ± 5 cm s^{-1}, respectively. In the benthic boundary layer (10 mab), the residual current had a predominant eastward orientation, which changed to south-southwest from May to October in 2015.

3.3 Acoustic backscatter

Acoustic backscatter in the lowest bin (2 -7 mab) of the LR-ADCP exhibited strong variation at short time scales (on the order of hours to weeks; Fig. 6A). The overall seasonal trend showed slightly lower values in February-March, that increased in April, parallel to the increase in chlorophyll a fluorescence (Fig. 6A). Hereafter, backscatter intensity remained high throughout summer, until a decrease occurred at the end of September. The latter was mirrored in the chlorophyll a fluorescence. Despite this

mirroring of the seasonal pattern in backscatter intensity and chlorophyll a fluorescence in the BBL, no covariance seemed to exist at shorter time scales of a few months (Fig. 7B). To assess the stability or temporary nature of a potential relationship of acoustic backscatter with chlorophyll fluorescence, local (in time) linear regressions were investigated on successive subsets of 2 weeks of data. The predictive power (R^2) of chlorophyll a fluorescence on variability in LR-ADCP backscatter intensity in the lowest bin peaked to 25% during the spring bloom, but varied between 0 and 7% for the rest of the year (Fig. 6B).

Similar analyses showed that bottom current speeds (here used as proxy for sediment resuspension) explained up to 27% of the variability in this backscatter intensity, but only in winter (Fig. 6B). Just as for the relationship with chlorophyll fluorescence, a global relationship over the entire season of backscatter intensity with current speed was not found.

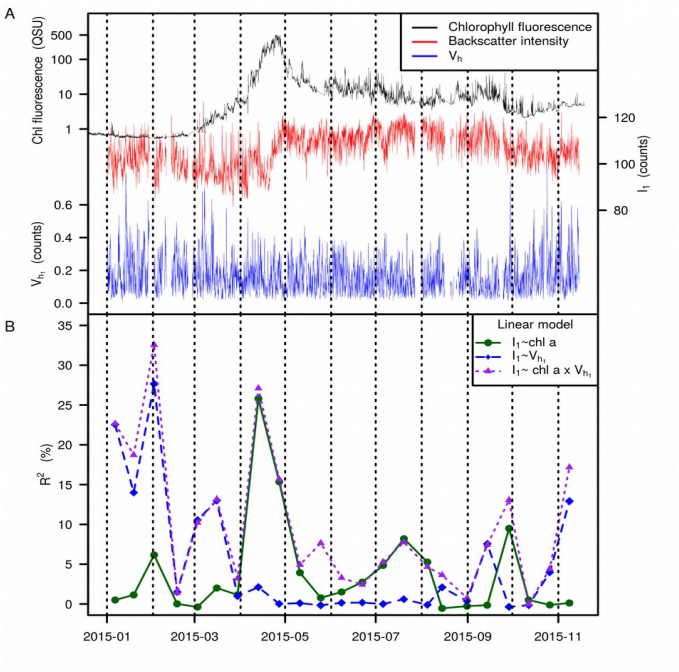

443 Fig. 6: Panel A: Time series of chlorophyll a fluorescence (log-scale), and acoustic backscatter (I_1) and
444 current speed (V_{h1}) in the bottom bin (2 – 7 mab) of the LR-ADCP. Panel B: R^2 (goodness-of-fit; %)
445 values from linear regression analyses performed on consecutive subsets of 2 weeks of LR-ADCP data
446 from the series in panel A. Linear regressions were performed with backscatter intensities (I) and
447 horizontal current speed (V_h; used as surrogate for turbidity) from the lowest bin (index 1 in legend)
448 and chlorophyll fluorescence (chl a) in the benthic boundary layer (log-transformed).
449

450 ***3.4 Phytoplankton bloom conditions at LoVe observatory***

451 The bottom chlorophyll increased from negligible fluorescence in winter to a peak in early May (Fig.
452 7A). The first visible fluorescence increases in figure 7A followed a peak in chlorophyll concentration
453 at the surface approximately one week earlier. However, a first very modest increase, which was only
454 visible in log-transformed fluorescence values, was already found early March (Fig. 6A).
455 After the spring bloom surface chlorophyll values and fluorescence in the benthic boundary layer were
456 more decoupled. Surface concentrations were still ~25% of those during the spring peak, while bottom
457 fluorescence was only ~5% of its peak value.
458 During the spring bloom (end of April – beginning of May), when the predictive power of chlorophyll
459 a fluorescence on variation in backscatter intensity was highest (Fig. 6B), increased backscatter

460 intensities extended from the surface down to the bottom (Fig. 7B). Similar backscatter features,
461 extending over the entire water column are discernible in mid-June, beginning of July, and mid-July in
462 figure 7B. Nevertheless, surface and bottom chlorophyll a signals seemed largely uncoupled
463 throughout summer in comparison to the spring peak.

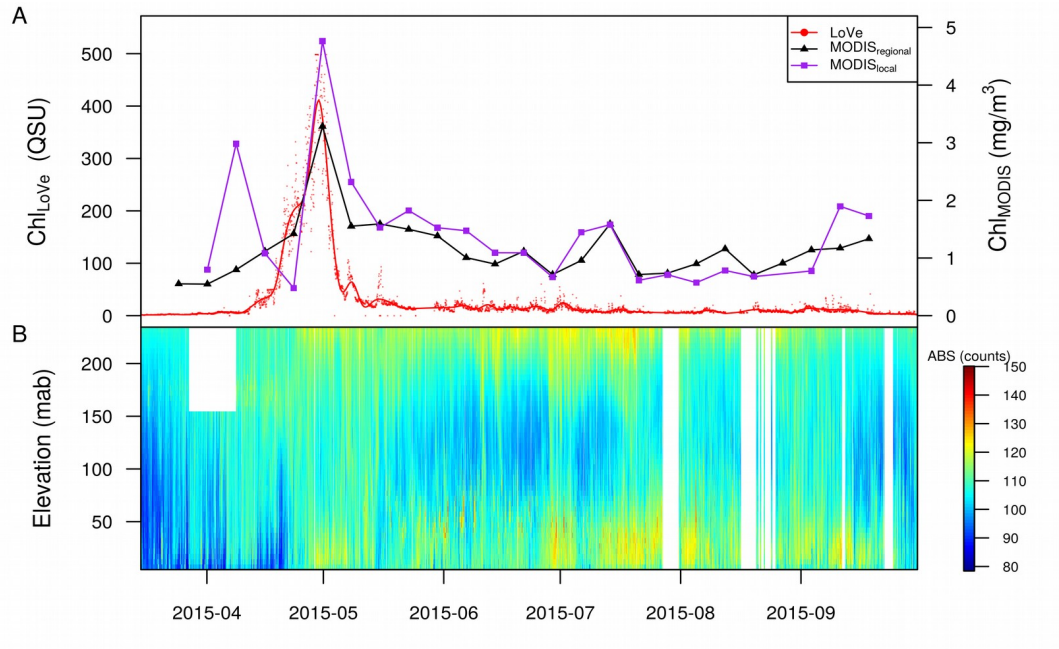

Fig. 7: Phytoplankton bloom conditions (A) and acoustic backscatter from the LR-ADCP (B) at LoVe observatory. Raw chlorophyll fluorescence (left axis in "Quantitative Scientific Units"; red line = smooth spline; dots = raw data) and surface chlorophyll concentrations from MODIS-Aqua (right axis; black triangles = regional; purple squares = local) show a consistent pattern throughout 2015.

3.5 Pre-bloom backscatter variability

No SR-ADCP data was available for spring 2015, so the backscatter intensity of both ADCPs and SIMRAD echosounder was compared for pre-bloom conditions during March 2014 (Fig. 8). The SR-ADCP (600 kHz) backscatter exhibited a few "descending" backscatter signals on March 3, 5 and 7 (Fig. 8C, lower) for which no corresponding backscatter patterns existed in the LR-ADCP (190 kHz; Fig. 8B) or echosounder data (70 kHz; Fig. 8A). Similar line patterns were also found in other parts of the time series, which at present we cannot explain.

From March 5 onwards, noise in the echosounder backscatter intensified at the surface (Fig. 8A), which can be attributed to bubble formation in stormy weather as indicated by the high wind speeds around that time (Fig. 3A). During this stormy period, patterns of increased echosounder backscatter emerged, that in some cases reached the bottom. The steepness of these backscatter features suggests strong

481 mixing during this time of the year (section 3.1). Similar backscatter excursions were found in the LR-
482 ADCP, but these were generally less pronounced (Fig. 8B). The SR-ADCP backscatter (Fig. 8C)
483 showed a sudden increase on March 5 and 6 that roughly corresponds to backscatter increases in the
484 LR-ADCP. During this stormy period both ADCPs showed increased backscatter at the bottom.

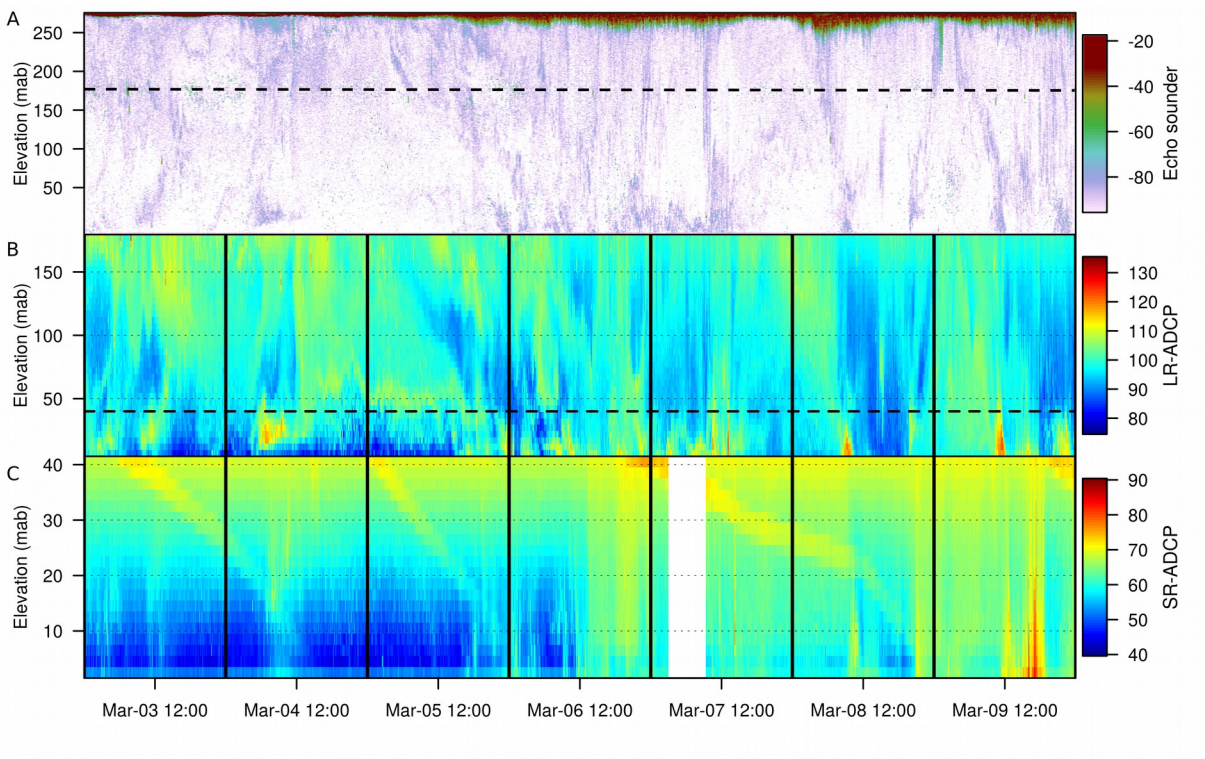

Fig. 8: Acoustic backscatter intensity from the echo sounder (A), the LR-ADCP (B), and the SR-ADCP (C) throughout the water column over time for the March 2014 (pre-bloom conditions). Intensities are in dB for the echo sounder, and in corrected counts for the ADCPs (Materials and methods). Horizontal dashed lines in the upper and middle graphs indicate the range of the instruments in the middle and lower graphs.

3.6 Post-bloom backscatter variability

A qualitative comparison of backscatter intensities among the ADCPs and echosounder during post-bloom conditions was made with data from July 2015 (Fig. 9). Above 150 mab, increased backscatter in the echosounder data reflected the presence of fish (blue-green colour; roughly -60 – -50 dB) and smaller material (roughly < -65 dB, purple; Fig. 9A). Below 100 mab, a clear up- and downward backscatter pattern with intensities between -60 and -50 dB was visible in the echosounder data, with a daily periodicity (Fig. 9A). The backscatter intensity ascended at the end of the day, and reached a maximal height above the bottom just before midnight. This backscatter signal descended towards the

seafloor during the late night and remained there during daytime. In the LR-ADCP data the migrating patterns of increased backscatter (roughly > 120 counts, red) were wider, and the echosounder patterns corresponded to the upper edges with highest intensities (> 130 counts, deep red; Fig. 9B). The SR-ADCP data again showed the migrating edges (> 75, yellow-red, Fig. 9C) from the LR-ADCP patterns, but the contrast with the background was weaker than in the echosounder profiles.

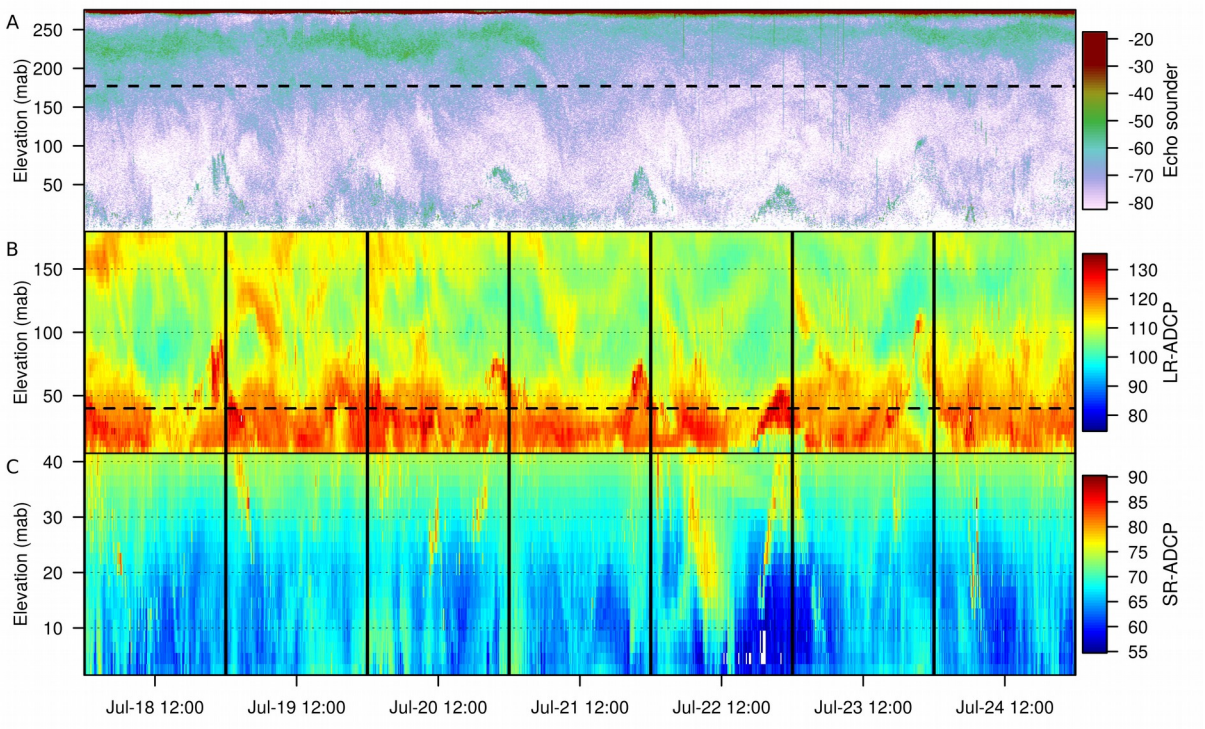

Fig. 9: Acoustic backscatter intensity from the echo sounder (upper), the LR-ADCP (middle), and the SR-ADCP throughout the water column over time for July 2015 (post-bloom conditions). Intensities are in dB for the echo sounder, and in corrected counts for the ADCPs (Materials and methods). Horizontal dashed lines in the upper and middle graphs indicate the range of the instruments in the middle and lower graphs.

4. Discussion

4.1 Residual water movement and organic matter origin

Available data suggest that the particulate organic matter (POM) arriving at the CWC of the LoVe observatory is likely of local origin. The horizontal residual transport at 10 and 100 mab is in the order of 5 – 10 cm s^{-1}. As surface currents could not be reliably estimated from the LR-ADCP readings, we assume a similar residual current for the upper part of the water column. This implies that POM is transported over distances of 4 – 10 km per day. Assuming further a passive settling velocity of 50 - 100 m d^{-1} for phytoplankton (Iversen and Ploug 2010) at the LoVe observatory (depth: ~260 m), the settling POM is likely produced within ~ 20 km from the station, i.e. within the Hola trough area and neighbouring coast. This is in line with the increased fluorescence over a trough relative to the

neighbouring banks reported for a region further North (Nordby et al. 1999). Nevertheless, the neighbouring bank, Vesterålsgrunnen, may also be a potentially important source of organic material via southward down-slope bottom currents (Fig. 4). The suggested local origin of the POM in the trough is further supported by particle tracking simulations that revealed a residence time of ~1 week for particles released in the surface layer (Silberberger et al. 2016). Based on primary production estimates of 130 g C m^{-2} y^{-1} from Skogen et al. (2007) and taking a surface area of 350 km^2 for the Hola trough (based on bathymetric data from the Mareano website: http://www.mareano.no), the total organic matter production is estimated at $45 \bullet 10^3$ tons C y^{-1}. Oxygen consumption rates measured at the Traena reef (Norway) using the aquatic eddy covariance method indicate an organic matter demand of CWC communities of 409 g C m^{-2} y^{-1} (Cathalot et al. 2015). With a surface area of 3.32 km^2 of CWCs in the Hola trough (based on visual classification of the bathymetric data from the Mareano website), the total CWC-reef organic matter demand in the Hola trough amounts to $1.4 \bullet 10^3$ tons C y^{-1}, which is equivalent to ~3 % of the total primary production above the trough. The export production for the northern troughs is estimated at 57 g C m^{-2} y^{-1} (Slagstad et al. 1999) or 43% of the total primary production. These rough estimates indicate that the local primary production and export into the Hola trough is sufficient to sustain the reef communities.

4.2 Hydrography and vertical transport

CWC communities depend on vertical transport of organic matter from surface primary production for their food supply (Thiem et al. 2006; Davies et al. 2009). Turbulent mixing is considered a key factor in this vertical transport on continental shelves and slopes (White et al. 2005; Wagner et al. 2011), but its strength depends on the governing hydrography. The hydrographic conditions at LoVe observatory

show considerable seasonal variation, consistent with earlier reported vertical profiles of salinity and temperature (Sundby 1984, Zhu et al. 2009). The water column is completely mixed in winter – spring. This was in our analysis reflected in the similarity between the temperature at the surface (derived from MODIS data) and the bottom (LoVe data). Bottom water salinity was during winter typical of a mixture of NAW (salinity typically ≥ 35) and NCW (salinity typically ≤ 34.5) water masses. The reason for this mixed signature is the progressive mixing of these water masses as they move northward towards the Barends Sea (Helland-Hansen and Nansen 1909, Pedersen et al. 2005). This is consistent with vertically homogeneous water column in terms of density as reported by Sundby (1984) for nearby troughs in spring, and the notion of a deep wedge-shaped NCC that take the form of a coastal jet in winter (Ikeda et al. 1988, Nordby et al. 1999, Sætre 2007, Skagseth et al. 2011). The lack of a density stratification, implies that there is little resistance against turbulent downwelling induced by the increased wind shear at this time of year. In addition, this coastal jet is known to produce mesoscale eddies in an interaction with bottom topography (Ikeda et al. 1988, Pedersen et al. 2005). Such eddies transport isolated packages of water with distinct temperature and/or salinity signatures, which (together with smaller scale turbulence) could explain our observed coherence between temperature and salinity signals at the LoVe observatory at scales up to a few weeks. It is understood that mesoscale eddies concentrate organic matter, harbour increased levels of biomass such as zooplankton and fish larvae, and transport it to deeper layers (Zhu et al. 2009, Godø et al. 2012a, Waite et al. 2016). Beside turbulent mixing and eddy-mediated downwelling, cooling-induced cascading (e.g. Ulses et al. 2008) of water masses from over the nearby bank could also explain the high coherence between bottom water salinity (BWS) and temperature (BWT). This is supported by the sudden decrease in sea surface temperature (SST) in February–March, at the beginning of the period of high coherence. Such cold-water cascading has been observed in canyons along the continental margin (Canals et al. 2006), and could provide an additional means of transport of organic matter produced above the nearby bank

566 towards the reef communities. Unfortunately, due to several periods of ADCP malfunctioning in early
567 spring, current velocity data are inconclusive to support this type of transport.
568
569 Towards summer, SST values increase substantially above the bottom water temperature as part of a
570 development of temperature stratification. This was verified by CTD casts during a maintenance cruise
571 in summer 2015, and corresponds with patterns reported by Zhu et al. (2009). Such a seasonal
572 stratification is common for the region and lasts until autumn. Stratification reduces turbulent
573 diffusivity and counteracts the vertical turbulent transport induced by wind shear. In addition, wind
574 stress decreases to a seasonal minimum in summer at the LoVe observatory. In the northern part of the
575 Norwegian continental shelf the summer minimum in wind stress seems to coincide with a minimum in
576 eddy kinetic energy (Andersson et al. 2011), and seasonality in wind forcing is considered a driver of
577 seasonality in the NCC (Skagseth et al. 2011). Although the distinction in water masses is less clear in
578 the northern part of the Norwegian continental shelf, the observed summer stratification fits within the
579 commonly accepted picture of a deep narrow coastal jet (NCC) in winter, that flattens to a layer of
580 NCW that covers the larger part of the continental shelf in summer, with somewhat denser NAW in the
581 trenches underneath (Nordby et al. 1999, Skagseth et al. 2011). The weakening of this coastal jet and
582 reduced turbulence can explain the absence of coherence between the bottom water temperature and
583 salinity in our analyses, and implies a reduced transport of surface organic matter to the reefs
584 throughout summer. This reduced vertical transport, together with lower primary production in the
585 surface layer, results in lower chlorophyll a fluorescence at the reefs, reflecting low phytodetritus
586 quantity and quality on the reefs. Note that the moderating role of hydrography for vertical transport
587 enhancement has important implication in a climate change context, since earlier and stronger water-
588 column stratification on the continental shelf (Holt et al. 2010) may shorten the period of intense
589 mixing, thus reducing the duration and intensity of phytodetritus supply to the benthic environment

590 (Järnegren and Kutti 2014).

591

592 ***4.3 Role of local hydrodynamics***

593 At LoVe observatory, tides are the dominant driver of water movement, with instantaneous current
594 speeds being roughly 3 - 5 times stronger than residual currents. The resulting shear stress may bring
595 and keep POM in suspension in the benthic boundary layer and make it more available to filter feeders
596 (Jones et al. 1998; Guihen et al. 2013; Davies et al. 2009). In addition, tidal currents enlarge the surface
597 area of the local primary production that can be filtered by the reef communities. Considering the
598 general counter-clockwise circulation in the Hola trough (Bøe et al. 2009) and the position of the
599 observatory relative to this circulation, the accessibility mainly extends towards the shelf break, where
600 primary production tends to be higher (Slagstad et al. 1999). Furthermore, tidal currents with diel
601 periodicity repeatedly 'pump' phytodetritus through the trough and hereby over the CWC reefs, which
602 increases the trapping efficiency of particulate material by the filter-feeding community. Hence, tidal
603 current dynamics not only act as an important transport component, but also as a catalyst for enhanced
604 trapping of the locally produced organic matter by the reef communities. This may partially
605 compensate for the lower supply from the surface and the lower nutritional quality of the phytodetritus
606 under stratified conditions.

607

608 ***4.4 A seasonal menu***

609 In winter, suspended matter concentrations are generally low, except during isolated storm events when
610 increased backscatter can be observed. The higher particle concentrations can be caused by sediment
611 resuspension, as indicated by the concurrent increases in bottom currents and relatively high
612 explanatory value of the local linear regression with horizontal current speed. However, initial

increases in fluorescence also coincided with this period of stormy weather. Indeed, phytoplankton production in winter and early spring (prior to the bloom) can also represent a substantial carbon export flux from the surface to the benthos during stormy weather (Thomsen et al. 2014), and appears to be more common than expected (e.g. Bishop and coworkers 2016). Particularly, the picoplankton grows all year long and may contribute to these early aggregates (Behrenfeld and Boss 2014). Nevertheless, the initial increase in fluorescence in March was not translated to substantial R^2 values for the regression of acoustic backscatter intensity with chlorophyll a fluorescence, suggesting that the acoustic backscatter in our data was mainly due to resuspended material. Increased turbidity during a resuspension event on March 9 and March 14 of 2014 were also observed in the still camera images from the observatory (Fig. 10). In summary, at the LoVe observatory stormy conditions in early spring can cause increased concentrations of suspended matter in the water column that mainly seems to consist of older resuspended material. However, small quantities of fresh phytoplankton/detritus from early production are present in the benthic boundary layer and may represent an important higher quality component of the available food to the reef communities, that is otherwise low in nutritional value this early in the season. *Lophelia pertusa* can tolerate extended periods of food deprivation by, albeit modest, reductions in its respiration rate (Larsson et al. 2013). However, the modest food supply may be of particular importance for the reproductive season, considering that Norwegian *L. pertusa* spawns in late winter (Waller 2005; Brooke and Järnegren 2013).

A 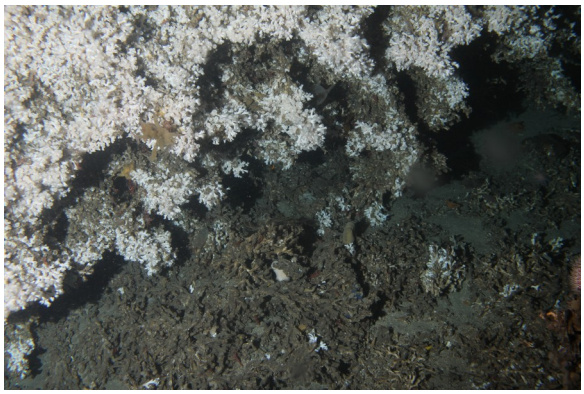 B 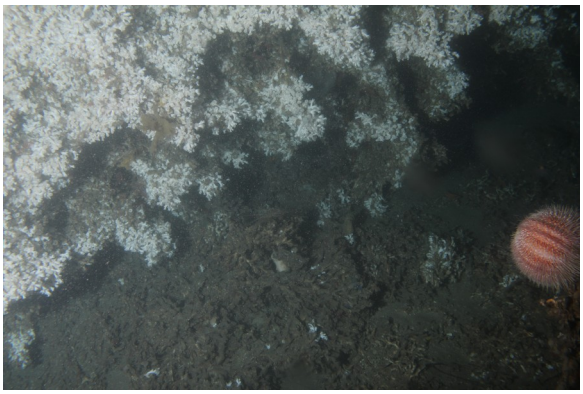

Fig. 10: Still camera images of the cold-water coral reef, dominated by *Lophelia pertusa*, near the satellite unit. The images were taken 3:31 UTC (A) and 17:19 UTC (B) on March 14, 2014. A resuspension event occurred in the afternoon, resulting in increased turbidity (B).

632

633

634 Phytoplankton biomass in surface waters near the observatory peaks in April – May (3 – 4.5 mg Chl m^{-3})
635 and during a secondary bloom in July (1.5 – 2 mg m^{-3}). Strong mixing rapidly transports the fresh
636 material to the BBL. The observed chlorophyll a fluorescence explained respectively up to 25% and
637 7% of the variability in backscatter intensity in the LR-ADCP bottom bin during these two periods,
638 indicating that phytodetritus contributed substantially to the suspended material in the BBL. The LR-
639 ADCP picked up pulses of vertical organic matter transport as repeated increases of backscatter
640 intensity throughout the entire water column during this bloom period, reflecting a strong surface-to-
641 bottom connectivity of high quality phytodetritus to the CWC reef communities.

642

643 Senescence of the spring bloom in the second half of May coincides with an increase of the SST above
644 the BWT and the development of water-column stratification, which impairs the downward transport of
645 surface-derived particulate material. This was supported by the low acoustic backscatter intensities at
646 mid-depth relative to the surface in summer and the entire water column during the periods of full
647 water-column mixing. In addition, the reduced connectivity between surface and bottom in summer

was manifested in the decoupling of two phytoplankton signals at the surface and near the bottom. The observed comparatively low chlorophyll fluorescence near the bottom in summer indicates that phytodetritus concentration and/or quality must have been substantially reduced near the CWC reefs relative to the spring mixing condition (Beaulieu 2002). Note, however, that chlorophyll sensors that measure at the 685nm wavelength can also respond to other optically active substances within the DOM pool. Fluorescence variability as measured by the fluorescence sensor may therefore not have a linear response to chlorophyll a dynamics. Still, several deep mixing events occurred during the stratification regime, when backscatter intensities temporarily increased again throughout the water column, hinting at a temporary coupling between surface and bottom. These are probably isolated eddies that still may originate from dynamic shelf waters. They have been previously identified from echosounder data as specific patterns of increased backscatter (Godø et al. 2012a), and may present important concentration and vertical transport mechanisms during a period of reduced vertical exchange (Waite et al. 2016).

In summer, when fresh phytodetritus at the seafloor was scarce, we observed a pronounced diurnal pattern of elevated acoustic backscatter intensity in the lower 100 meters of the water column, which suggests that migrating organisms were a dominant source of backscatter. Migration patterns above CWC reefs were also reported for the Gulf of Mexico (Davies et al. 2010; Mienis et al. 2012). The migration patterns in backscatter intensity between -60 and -50 dB in the calibrated echosounder were also pickup by the SR-ADCP and can be attributed to fish. However, the broader patterns in the LR-ADCP, of which the upper edge corresponds to the migration patterns in the echosounder and SR-ADCP, suggest that an additional source of backscatter must have been present. The scattering model of Lavery et al. (2007) suggests that this scattering source, with a high sensitivity at 190 kHz (LR-ADCP), but low sensitivity at 70 kHz (echosounder) and 600 kHz (SR-ADCP), may well correspond to

euphausiids. Several studies have indicated that zooplankton can be an important food source for cold-water corals at least for a part of the year (Kiriakoulakis et al. 2005; Naumann et al. 2011; Orejas et al. 2016) and feed on whatever zooplankton is available, which can vary spatially and temporally (Dodds et al. 2009). Zooplankton is hypothesized to present an important food source in permanently stratified tropical (Hebbeln et al. 2014) and oligotrophic waters (Carlier et al. 2009). Lipid analyses have pointed out that particularly copepods are readily taken up by cold-water corals and can at times be their primary food source at the North-East Atlantic margin (Kiriakoulakis et al. 2005). Both copepods and euphausiids have been used in feeding experiments (e.g. Dodds et al. 2007; Orejas et al. 2016), and both can be part of the natural CWC diet (Dodds et al. 2009; Khripounoff et al. 2014). The specific backscatter profiles suggest that the migrating zooplankton were most likely euphausiids, while indications for copepod migration – which should be visible in the SR-ADCP acoustics (600 kHz; Lavery et al. 2007) – were not found.

Meganyctiphanes norvegica, one of the most abundant euphausiid species on the Norwegian shelf, is an opportunistic omnivorous feeder that, depending on food availability, can shift between benthic feeding on mainly phytodetritus and a more carnivorous lifestyle with diurnal vertical migration (Schmidt 2010). The absence of copepods in the backscatter signal of the SR-ADCP could be caused by avoidance behaviour of the copepods towards their potential predator, *M. norvegica*, which can reside close to the bottom during daytime (Falk-Petersen et al. 2000; Dalpadado 2006; Schmidt 2010). The copepods may therefore have been out of range of the SR-ADCP. Although we lack zooplankton surveys for backscatter calibration and ground-truthing, our observations are inline with a vertical migration after the spring bloom by zooplankton. This zooplankton migration is not a direct evidence of zooplankton feeding by CWC or associated fauna, but polyp feeding activity of *L. pertusa* increased from the beginning of May (Osterloff et al. 2016a).

Zooplankton has been shown to comprise a substantial part of the cold-water coral diet in oligotrophic regions (Carlier et al. 2009). CWC feeding on zooplankton at the LoVe observatory throughout summer would compensate for the scarcity of fresh phytodetritus in the lower part of the Hola trough during summer in two ways, and explain the comparatively high zooplankton diet contribution for the nearby Traena communities (Van Oevelen et al. 2018). Firstly, diurnally migrating zooplankton grazes in the upper water column at night and bridges the distance that passively sinking organic matter has to travel to reach the BBL. In addition, fecal pellets tend to sink fast and may provide another form of flux enhancement (Youngbluth et al. 1989). This zooplankton-mediated transport of organic matter is also less dependent on water column mixing, since diurnal vertical migration behaviour does not depend on stratification conditions (Baumgartner et al. 2011). Secondly, zooplankton grazing may act as an intermediate step that upgrades the nutritional value of the CWC diet by concentrating particular elements or nutritional components. For example, the similarity in C/N ratio between CWCs and zooplankton (e.g. Mueller et al. 2014) may increase the efficiency of N acquisition by the CWCs and compensate for the higher C/N ratio that is generally observed for aged phytodetritus (e.g. Beaulieu 2002). Zooplankton is also richer in poly-unsaturated fatty acids (PUFAs) than sinking detritus and may present an essential PUFA source to benthic communities (e.g. Tiselius et al. 2012). Such an upgrade in food quality would compensate for the deteriorating quality of the algal material throughout summer, particularly in the case of *M. norvegica* which is known to be predominantly phytophagous in spring and summer (Schmidt 2010). A similar seasonal succession in coral diet was also suggested for corals living in a canyon in the Bay of Biscay (Khripounoff et al. 2014).

5. Conclusions

Ocean observatories are a means to elucidate oceanic processes over extended spatial scales. In this study, data from a new observatory on the Norwegian continental shelf were used to shed light on the

seasonal importance of physical and biological drivers of a nearby cold-water coral reef.

CWC reefs in the Hola trough receive organic matter from local primary production that is mixed down to the bottom by strong turbulence. However, water-column mixing is reduced in summer due to stratification, resulting in an impaired supply of phytodetritus to the reef communities.

Horizontal currents are predominantly tidally driven in the trough and enhance the accessibility of organic matter to the reef communities by extending the horizontal range of organic matter transport to the larger part of the trough. The consistency in current direction and repetitive character of the currents probably enhances the capturing efficiency of the filter feeders by repeatedly flushing phytodetritus past the reef communities.

Our results suggest that the reduced supply of fresh phytodetritus in summer at the Lofoten-Vesterålen observatory is compensated by a seasonal succession in food type. Vertically migrating zooplankton may counterbalance the observed lower phytodetritus availability in summer by shunting passive vertical transport of fresh organic material and upgrading the nutritional value of the food for the filter feeders. Food deprivation seemed to be limited to the non-productive winter season, when only storm-induced resuspension of (low quality) particles into the bottom water.

Although many of the investigated signals did not provide direct quantitative evidence, for instance due to absence of calibrations and ground-truth data, a consistent picture emerged by combining different sources of information. Studies like the one presented can provide a valuable basis to give direction to more dedicated in-depth campaigns. Our study contributes to a growing body of literature that illustrates the vast potential of large permanent research infrastructure like the LoVe observatory.

744

745 **Appendix: Data quality of the Lofoten-Vesterålen ocean observatory (Statoil)**

746

747 **References**

748 Andersson, M., K.A. Orvik, J.H. LaCasce, I. Koszalka, C. Mauritzen. 2011. Variability of the
749 Norwegian Atlantic Current and associated eddy field from surface drifters. Journal of
750 Geophysical Research, 116: C08032, doi:10.1029/2011JC007078

751

752 Baumgartner M.F., Lysiak N.S.J., Schuman C., Urban-Rich J., Wenzel F.W. 2011. Diel vertical
753 migration behavior of *Calanus finmarchicus* and its influence on right and sei whale occurrence.
754 Marine Ecology-Progress Series, 423: 167-184

755

756 Beaulieu, S.E. 2002. Accumulation and fate of phytodetritus on the sea floor. In: Gibson R. N. , Barnes
757 M., and R. J. A. Atkinson (eds.). Oceanography and Marine Biology: Annual Review. 40: 171-
758 232

759

760 Behrenfeld, M.J., Boss, E.S., 2014. Resurrecting the ecological underpinnings of ocean plankton
761 blooms. Ann. Rev. Mar. Sci. 6, 167–194. https://doi.org/10.1146/annurev-marine-052913-
762 021325.

763

764 Bishop, J.K., Fong, M.B., Wood, T.J., 2016. Robotic observations of high wintertime carbon export in
765 California coastal waters. Biogeosciences 13, 3109–3129. https://doi.org/10.5194/bg-13-3109-
766 2016.

767

768 Bloomfield, P. 2000. Fourier analysis of time series: an introduction, 2nd edition. Wiley & Sons, New
769 York pp. 288

770

771 Bøe R., V.K. Bellec, M.F.J. Dolan, P. Buhl-Mortensen, L. Buhl-Mortensen, D. Slagstad, L. Rise. 2009.
772 Giant sandwaves in the Hola glacial trough off Vesterålen, North Norway. Marine Geology, 267:
773 36-54

774
775 Brooke, S., J. Järnegren. 2013. Reproductive periodicity of the scleractinian coral *Lophelia pertusa*
776 from the Trondheim Fjord, Norway. Marine Biology 160: 139-153, doi:10.1007/s00227-012-
777 2071-x
778
779 Buhl-Mortensen, L., R. Bøe, M.F. Dolan, P. Buhl-Mortensen, T. Thorsnes, S. Elvenes, H. Hodnesdal.
780 2012. Banks, troughs and canyons on the continental margin off Lofoten, Vesterålen, and Troms,
781 Norway. Seafloor Geomorphology as Benthic Habitat: GeoHab Atlas of Seafloor Geomorphic
782 Features and Benthic Habitats. Elsevier Insights, London. doi:10.1016/B978-0-12-385140-
783 6.00051-7
784
785 Canals, M., P. Puig, X. Durrieu de Madron, S. Heussner, A. Palanques, J. Fabres. 2006. Flushing
786 submarine canyons. Nature 444: 354–357, doi:10.1038/nature05271
787
788 Carlier, A., E. Le Guilloux, K. Olu, J. Sarrazin, F. Mastrototaro, M. Taviani, J. Clavier. 2009. Trophic
789 relationships in a deep Mediterranean cold-water coral bank (Santa Maria di Leuca, Ionian Sea).
790 Marine Ecology-Progress Series 397:125-137, doi:10.3354/meps08361
791
792 Cathalot, C., D. Van Oevelen, T.J.S. Cox, T. Kutti, M. Lavaleye, G. Duineveld, F.J.R. Meysman. 2015.
793 Cold-water coral reefs and adjacent sponge grounds: hotspots of benthic respiration and organic
794 carbon cycling in the deep sea. Frontiers in Marine Science, 2:37, doi:10.3389/fmars.2015.00037
795
796 Constantine, W., D.B. Percival. 2013. wmtsa: Wavelet Methods for Time Series Analysis. R package
797 version 2.0-0. https://CRAN.R-project.org/package=wmtsa
798
799 Correa, T.B.S, G.P. Eberli, M. Grasmueck, J.K. Reed, A.M.S. Correa. 2012. Genesis and morphology
800 of cold-water coral ridges in a unidirectional current regime. Marine Geology, 326-328: 14-27,
801 doi:10.1016/j.margeo.2012.06.008
802
803 Cyr, F., H. van Haren, F. Mienis, G. Duineveld, D. Bourgault. 2016. On the influence of cold-water
804 coral mound size on flow hydrodynamics, and vice versa. Geophysical Research Letters, 43: 775-

783, doi:10.1002/2015GL067038

Dalpadado, P. 2006. Distribution and reproduction strategies of krill (Euphausiacea) on the Norwegian shelf. Polar Biology, 29: 849, doi:10.1007/s00300-006-0123-8

Daubechies, I. 1992. Ten lectures on wavelets. Society for Industrial and Applied Mathematics, Philadelphia, PA, USA: pp. 369

Davies, A.J., G.C.A Duineveld, M.S.S Lavaleye, M.J.N. Bergman, H. van Haren. 2009. Downwelling and deep-water bottom currents as food supply mechanisms to the cold-water coral *Lophelia pertusa* (Scleractinia) at the Mingulay Reef complex. Limnology and Oceanography, 54(2): 620-629

Davies, A.J., G.C.A. Duineveld, T.C.E. van Weering, F. Mienis, A.M. Quattrini, H.E. Seim, J.M. Bane, S.W. Ross. 2010. Short-term environmental variability in cold-water coral habitat at Viosca Knoll, Gulf of Mexico. Deep Sea Research Part I: Oceanographic Research Papers, 57: 199-212, doi:10.1016/j.dsr.2009.10.012

De Clippele, L.H., P. Buhl-Mortensen, L. Buhl-Mortensen. 2015. Fauna associated with cold water gorgonians and sea pens. Continental Shelf Research, 105: 67-78

De Mol, B., P. Van Rensbergen, S. Pillen, K. Van Herreweghe, D. Van Rooij, A. McDonnell, V. Huvenne, M. Ivanov, R. Swennen, J.P. Henriet. 2002. Large deep-water coral banks in the Porcupine Basin, southwest of Ireland. Marine Geology, 188: 193-231, doi:10.1016/S0025-3227(02)00281-5

de Goeij, J.M., D. van Oevelen, M.J.A. Vermeij, R. Osinga, J.J. Middelburg, A.F.P.M. de Goeij, W. Admiraal. 2013. Surviving in a Marine Desert: The Sponge Loop Retains Resources Within Coral Reefs. Science, 342: 108-110, doi:10.1126/science.1241981

Dodds, L.A., J.M. Roberts, A.C. Taylor, F. Marubini. 2007. Metabolic tolerance of the cold-water coral *Lophelia pertusa* (Scleractinia) to temperature and dissolved oxygen change. Journal of

Experimental Marine Biology and Ecology 349: 205-214, doi:10.1016/j.jembe.2007.05.013

Dodds, L.A., K.D. Black, H. Orr, J.M. Roberts. 2009. Lipid biomarkers reveal geographic differences in food supply to the cold-water coral *Lophelia pertusa* (Scleractinia). Marine Ecology Progress Series, 397: 113-124, doi:10.3354/meps08143

Downing, A., P.D. Thorne, C.E. Vincent. 1995. Backscattering from a suspension in the near field of a piston transducer. Journal of the Acoustic Society of America 97(3): 1614-1620

Duineveld, G.C.A, M.S.S Lavaleye, M.J.N. Bergman, H. de Stigter, F. Mienis. 2007. Trophic structure of a cold-water corral mound community (Rockall Bank, NE Atlantic) in relation to the near-bottom particle supply and current regime. Bulletin of Marine Science, 81(3): 449-467

Duineveld, G.C.A., R.M. Jeffreys, M.S.S. Lavaleye, A.J. Davies, M.J.N. Bergman, T. Watmough, R. Witbaard. 2012. Spatial and tidal variation in food supply to shallow cold-water coral reefs of the Mingulay Reef complex (Outer Hebrides, Scotland). Marine Ecology Progress Series, 444: 97-115, doi:10.3354/meps09430

Ersdal, G. 2001. An overview of ocean currents with emphasis on currents on the Norwegian continental shelf. NPD Preliminary Report, March 2001, 40 pp.

Falk-Petersen, S., W. Hagen, G. Kattner, A. Clarke, J. Sargent. 2000. Lipids, trophic relationships, and biodiversity in Arctic and Antarctic krill. Canadian Journal of Fisheries and Aquatic Sciences, 57:178-191, doi:10.1139/f00-194

Findlay, H.S., Y. Artioli, J. Moreno Navas, S.J. Hennige, L.C. Wicks, V.AI. Huvenne, E.M.S. Woodward, J.M. Roberts. 2013. Tidal downwelling and implications of future ocean acidification and warming on cold-water coral reefs. Global Change Biology, 19: 2708-2719, doi:10.1111/gcb.12256

Foote, K.G., H.P. Knudsen, G. Vestnes, D.N. MacLennan, E.J. Simmonds. 1987. Calibration of acoustic instruments for fish density estimation: a practical guide, ICES Coop. Res. Rep. 144.

Fosså, J.H., P.B. Mortensen, D.M. Furevik. 2002. The deep-water coral *Lophelia pertusa* in Norwegian waters: distribution and fishery impacts. Hydrobiologia, 471: 1-12

Godø O.R., A. Samuelsen, G.J. Macaulay, R. Patel, S.S. Hjøllo, J. Horne, S. Kaartveldt, J.A. Johannessen. 2012a. Mesoscale eddies are oases for higher trophic marine life. PLoS ONE 7: e30161, doi:10.1371/journal.pone.0030161

Godø, O.R., E. Tenningen, M. Ostrowski, R. Kubilius, T. Kutti, R. Korneliussen, J.H. Fosså. 2012b. The Hermes Lander project – the technology, the data, and the evaluation of concept and results. Report nr. 3/2012.

Godø, O.R., S. Johnsen, T. Torkelsen. 2014. The love ocean observatory is in operation. Marine Technology Society Journal, 48: 24-30.

Gori, A., R. Grover, C. Orejas, S. Sikorski, C. Ferrier-Pages. 2014. Uptake of dissolved free amino acids by four cold-water coral species from the Mediterranean Sea. Deep-Sea Research Part II, 99: 42–50

Gori, A., S. Reynaud, C. Orejas, C. Ferrier-Pagès. 2015. The influence of flow velocity and temperature on zooplankton capture rates by the cold-water coral *Dendrophyllia cornigera*. Journal of Experimental Marine Biology and Ecology, 466: 92-97, doi:10.1016/j.jembe.2015.02.004

892

893 Gostiaux, L., H. van Haren. 2010. Extracting meaningful information from uncalibrated backscatter
894 echo intensity data. Journal of Atmospheric and Oceanic Technology, 27: 943–949.
895 doi:10.1175/2009JTECHO704.1

896

897 Gouhier, T.C. , A. Grinstead and V. Simko. 2016. biwavelet: Conduct univariate and bivariate wavelet
898 analyses (Version 0.20.10). Available from http://github.com/tgouhier/biwavelet

899

900 Guihen, D., M. White, T. Lundälv. 2013. Boundary layer flow dynamics at a cold-water coral reef.
901 Journal of Sea Research, 78: 36-44, doi:10.1016/j.seares.2012.12.007

902

903 Hays, G.C. 2003. A review of the adaptive significance and ecosystem consequences of zooplankton
904 diel vertical migrations. In: Jones M.B., A. Ingólfsson, E. Ólafsson, G.V. Helgason, K.
905 Gunnarsson, J. Svavarsson (eds) Migrations and Dispersal of Marine Organisms. Developments
906 in Hydrobiology, 174. Springer, Dordrecht

907

908 Hebbeln, D., C. Wienberg, P. Wintersteller, A. Freiwald, M. Becker, L. Beuck, C. Dullo, G.P. Eberli,
909 S. Glogowski, L. Matos, N. Forster, H. Reyes-Bonilla, M. Taviani. 2014. Environmental forcing
910 of the Campeche cold-water coral province, southern Gulf of Mexico. Biogeosciences, 11: 1799-
911 1815

912

913 Helland-Hansen, B., F. Nansen. 1909. The Norwegian Sea. Its physical oceanography based upon the
914 Norwegian researches 1900–1904. Report on Norwegian Fishery and Marine Investigations, 2,
915 pp. 390

916

917 Holt, J., S. Wakelin, J. Lowe, J. Tinker. 2010. The potential impacts of climate change on the

hydrography of the northwest European continental shelf. Progress in Oceanography, 86: 361-379, doi:10.1016/j.pocean.2010.05.003

Huvenne, V.A.I., P.A. Tyler, D.G. Masson, E.H. Fisher, C. Hauton, V. Hühnerbach, T.P. Le Bas, G.A. Wolff. 2011. A picture on the wall: innovative mapping reveals cold-water coral refuge in submarine canyon. PLOS ONE, 6: e28755, doi:10.1371/journal.pone.0028755

Ikeda, M., J.A. Johannessen, K. Lygre, S. Sandven. 1988. A process study of mesoscale meanders and eddies in the Norwegian Coastal Current. Journal of Physical Oceanography, 19: 20-35

Iversen, M. H., H. Ploug. 2010. Ballast minerals and the sinking carbon flux in the ocean: carbon-specific respiration rates and sinking velocity of marine snow aggregates. Biogeosciences, 7: 2613–2624, doi:10.5194/bg-7-2613-2010

Järnegren, J., T. Kutti. 2014. *Lophelia pertusa* in Norwegian waters. What have we learned since 2008? - NINA Report 1028: 40 pp.

Jones, S.E., C.F. Jago, A.J. Bale, D. Chapman, R.J.M. Howland, J. Jackson. 1998. Aggregation and resuspension of suspended particulate matter at a seasonally stratified site in the southern North Sea: physical and biological controls. Continental Shelf Research 18: 1283-1309

Korneliussen, R.J., Y. Heggelund, G.J. Macaulay, D. Patel, E. Johnsen, I.K. Eliassen. 2016. *Acoustic identification of marine species using a feature library*. Methods in Oceanography, 17: 187–205

Khripounoff, A., J.-C. Caprais, J. Le Bruchec, P. Noel, C. Cathalot. 2014. Deep cold-water coral ecosystems in the Brittany submarine canyons (Northeast Atlantic): Hydrodynamics, particle supply, respiration, and carbon cycling. Limnology and Oceanography, 59(1): 87-98

Kiriakoulakis, K., Fisher E., Wolff G.A., Freiwald A., Grehan A., Roberts J.M. 2005. Lipids and nitrogen isotopes of two deep-water corals from the North-East Atlantic: initial results and implication for their nutrition, in: Freiwald A., Roberts J.M. (Eds.), Cold-water corals and

ecosystems. Springer-Verlag, Berlin Heidelberg, pp. 715-729

Larsson, A.I., T. Lundälv, D. Van Oevelen. 2013. Skeletal growth, respiration rate and fatty acid composition in the cold-water coral Lophelia pertusa under varying food conditions. Marine Ecology Progress Series, 483: 169-184

Lavaleye, M., G. Duineveld, T. Lundälv, M. White, D. Guihen, K. Kiriakoulakis, G.A. Wolff. 2009. Cold-water corals on the Tisler reef: Preliminary observations on the dynamic reef environment. Oceanography 22(1): 76–84, http://dx.doi.org/10.5670/oceanog.2009.08

Lavery, A.C., P.H. Wiebe, T.K. Stanton, G.L. Lawson, M.C. Benfield, N. Copley. 2007. Determining dominant scatterers of sound in mixed zooplankton populations. The Journal of the Acoustical Society of America, 122: 3304-3326, doi:10.1121/1.2793613

Mallat, S. (1999). A wavelet tour of signal processing. Academic Press, San Diego, USA: pp. 637

Mohn, C., A. Rengstorf, M. White, G. Duineveld, F. Mienis, K. Soetaert, A. Grehan. 2014. Linking benthic hydrodynamics and cold-water coral occurrences: A high-resolution model study at three cold-water coral provinces in the NE Atlantic. Progress in Oceanography, 122: 92-104, doi:10.1016/j.pocean.2013.12.003

Mienis, F., H.C. de Stigter, M. White, G. Duineveld, H. de Haas, T.C.E. van Weering. 2007. Hydrodynamic controls on cold-water coral growth and carbonate-mound development at the SW and SE Rockall Trough Margin, NE Atlantic Ocean. Deep-Sea Research I, 54: 1655-1674

Mienis, F., G.C.A. Duineveld, A.J. Davies, S.W. Ross, H. Seim, J. Bane, T.C.E. van Weering. 2012. The influence of near-bed hydrodynamic conditions on cold-water corals in the Viosca Knoll area, Gulf of Mexico. Deep Sea Research Part I: Oceanographic Research Papers, 60: 32-45, doi:10.1016/j.dsr.2011.10.007

Mueller, C.E., A.I. Larsson, B. Veuger, J.J. Middelburg, D. van Oevelen. 2014. Opportunistic feeding

on various organic food sources by the cold-water coral *Lophelia pertusa*. Biogeosciences, 11: 123-133

Nordby, E., K.S. Tande, H. Svendsen, D. Slagstad. 1999. Oceanography and fluorescence at the shelf break off the north Norwegian coast (69°20'N-70°30'N) during the main productive period in 1994. Sarsia, 84:175-189

OBPG. 2017. NASA Goddard Space Flight Center, Ocean Ecology Laboratory, Ocean Biology Processing Group. Moderate-resolution Imaging Spectroradiometer (MODIS) Aqua Level-3 Mapped Chlorophyll Data Version 2014; NASA OB.DAAC, Greenbelt, MD, USA. doi:10.5067/AQUA/MODIS/L3M/CHL/2014. Accessed on 02/17/2017

Naumann, M.S., C. Orejas, C. Wild, C. Ferrier-Pagès. 2011. First evidence for zooplankton feeding sustaining key physiological processes in a scleractinian cold-water coral. Journal of Experimental Biology, 214: 3570-3576, doi:10.1242/jeb.061390

Osterloff J., Nilssen I., Järnegren J., Buhl-Mortensen P., Nattkemper T.W. 2016a. Polyp activity estimation and monitoring for cold water corals with a deep learning approach. In: Proceedings of CVAUI 2016 (ICPR Workshop), Cancun, Mexico.

Osterloff, J., I. Nilssen, T.W. Nattkemper. 2016b. A computer vision approach for monitoring the spatial and temporal shrimp distribution at the LoVe observatory. Methods in Oceanography, 15: 114-128

Orejas, C., A. Gori, C. Rad-Menéndez, K.S. Last, A.J. Davies, C.M. Beveridge, D. Sadd, K. Kiriakoulakis, U. Witte, J.M. Roberts. 2016. The effect of flow speed and food size on the capture efficiency and feeding behaviour of the cold-water coral *Lophelia pertusa*. Journal of Experimental Marine Biology and Ecology, 481: 34-40, doi:10.1016/j.jembe.2016.04.002

Pedersen, O. P., M. Zhou, K.S. Tande, A. Edvardsen. 2005. Eddy formation on the coast of North Norway - evidenced by synoptic sampling. ICES Journal of Marine Science, 62: 615-628

Percival, D.B., A.T Walden. 2000. Wavelet methods for time series analysis. Cambridge University Press, Cambridge, UK: pp. 594

Purser, A., A.I. Larsson, L. Thomsen, D. van Oevelen. 2010. The influence of flow velocity and food concentration on *Lophelia pertusa* (Scleractinia) zooplankton capture rates. Journal of Experimental Marine Biology and Ecology, 395: 55-62

R Core Team. 2016. R: A language and environment for statistical computing. R Foundation for Statistical Computing, Vienna, Austria. URL https://www.R-project.org/.

Roberts, J.M., O.C. Peppe, L.A. Dodds, D.J. Mercer, W.T. Thomson, J.D. Gage, D.T. Meldrum. 2005. Monitoring environmental variability around cold-water coral reefs: the use of benthic photolander and the potential of seafloor observatories. In Cold-Water Corals and Ecosystems (eds.) A. Freiwald , J.M. Roberts. Springer, Berlin: 483-502

Roberts, J.M., A.J Wheeler, A. Freiwald. 2006. Reefs of the deep: The biology and geology of cold-water coral ecosystems. Science, 312: 543-547

Rovelli, L., K.M. Attard, L.D. Bryant, S. Flögel, H. Stahl, J.M. Roberts, P. Linke, R.N. Glud. 2015. Benthic O2 uptake of two cold-water coral communities estimated with the non-invasive eddy correlation technique. Marine Ecology Progress Series, 525: 97-104, doi:10.3354/meps11211

Sætre, R. (Ed.) 2007. The Norwegian Coastal Current - Oceanography and climate, Tapir Academic Press, Trondheim, Norway.

Schmidt K. 2010. Food and feeding in northernkrill (*Meganyctiphanes norvegica* (Sars), in: Tarling G.A. (Ed.), Advances in Marine Biology. Academic Press, pp. 127-171

Shumway, R.H., D.S. Stoffer. 2006. Time series analysis and its applications. Springer, New York, pp. 576, doi:10.1007/0-387-36276-2

Silberberger, M.J., P.E. Renaud, B. Espinasse, H. Reiss. 2016. Spatial and temporal structure of the meroplankton community in a sub-Artic shelf system. Marine Ecology-Progress Series, 555: 79-93.

Skagseth, Ø., K. F. Drinkwater, and E. Terrile. 2011. Wind- and buoyancy-induced transport of the Norwegian Coastal Current in the Barents Sea. Journal of Geophysical Research 116: C08007, doi:10.1029/2011JC006996

Skogen, M.D., W.P. Budgell, F. Rey. 2007. Interannual variability in Nordic seas primary production. ICES Journal of Marine Science, 64: 889-898, doi: 10.1093/icesjms/fsm063

Slagstad, D., K.S. Tande, P. Wassman. 1999. Modelled carbon fluxes as validated by field dta on the north Norwegian shelf during the productive period in 1994. Sarsia, 84: 303-317, doi:10.1080/00364827.1999.10420434

Soetaert, K., C. Mohn, A. Rengstorf, A. Grehan, D. van Oevelen. 2016. Ecosystem engineering creates a direct nutritional link between 600-m deep col-water coral mounds and surface productivity. Scientific reports 6: 35057

Soltwedel, T., E. Bauerfeind, M. Bergmann, N. Budaeva, E. Hoste, N. Jaeckisch, K. von Juterzenka, J. Matthiessen, V. Mokievsky, E.-M. Nöthig, N.-V. Quéric, R. Sablotny, E. Sauter, I. Schewe, B. Urban-Malinga, J. Wegner, M. Wlodarska-Kowalczuk, M. Klages. 2005. HAUSGARTEN: Multidisciplinary investigations at a deep-sea, long-term observatory in the Arctic Ocean. Oceanography 18: 46-61

Sundby, S. 1984. Influence of bottom topography on the circulation at the continental shelf off northern Norway. FiskDir. Skr. Ser. HavUnders. 17: 501-519

Thiem, Ø., E. Ravagnan, J.H. Fosså, J. Berntsen. 2006. Food supply mechanisms for cold-water corals along a continental shelf edge. Journal of Marine Systems, 60: 207-219

Tiselius, P., B.W. Hansen, D. Calliari. 2012. Fatty acid transformation in zooplankton: from seston to benthos. Marine Ecology-Progress Series, 446: 131-144

Torrence, C., G.P. Compo. 1998. A practical guide to wavelet analysis. Bulletin of the American Meteorological Society, 79: 61–78, doi:10.1175/1520-0477

Thomsen, L., Aguzzi, J., Costa, C., De Leo, F., Ogston, A., Purser, A., 2017. The oceanic biological pump: rapid carbon transfer to depth at continental margins during winter. Scientific reports 7, 10763. https://doi.org/10.1038/s41598-017-11075-6.

Ulses, C., C. Estournel, J. Bonnin, X. Durrieu de Madron, P. Marsaleix. 2008. Impact of storms and dense water cascading on shelf-slope exchanges in the Gulf of Lion (NW Mediterreanean). Journal of Geophysical Research, 113: C02010, doi:1029/2006JC003795

Van Oevelen, D., G.C.A. Duineveld, M.S.S. Lavaleye, F. Mienis, K. Soetaert, C.H.R. Heip. 2009. The cold-water coral community as hotspot of carbon cycling on continental margins: a food web analysis from Rockall Bank (northeast Atlantic). Limnology and Oceanography 54: 1829-1844

Van Oevelen, D., G.C.A. Duineveld, M.S.S Lavaleye, T. Kutti, K. Soetaert. 2018. Trophic structure of cold-water coral communities revealed from the analysis of tissue isotopes and fatty acid composition. Marine Biology Research 14(3):1-20, doi: 10.1080/17451000.2017.1398404

Van Weering, T.C.E., H. de Haas, H.C. de Stigter, H. Lykke-Andersen, I. Kouvaev. 2003. Structure and development of giant carbonate mounds at the SW and SE Rockall Trough margins, NE Atlantic Ocean. Marine Geology, 198: 67-81, doi:10.1016/S0025-3227(03)00095-1

Wagner, H., A. Purser, L. Thomsen, C.C. Jesus, T. Lundälv. 2011. Particulate organic matter fluxes and hydrodynamics at the Tisler cold-water coral reef. Journal of Marine Systems 85: 19-29

Waite A.M., L. Stemmann, L. Guidi, P.H.R. Calil, A.M.C. Hogg, M. Feng, P.A. Thompson, M. Picheral, G. Gorsky. 2016. The wineglass effect shapes particle export to the deep ocean in

mesocale eddies. Geophysical Research Letters 43, 9791 – 9800, doi:10.1002/2015GL066463

Waller, R.G. 2005. Deep-water Scleractinia (Cnidaria: Anthozoa): current knowledge of reproductive processes. In A. Freiwald and J. M. Roberts [eds.]. Cold-water corals and ecosystems. Springer-Verlag: 691-700

Whitcher, B. 2015. waveslim: Basic wavelet routines for one-, two- and three-dimensional signal processing. R package version 1.7.5. https://CRAN.R-project.org/package=waveslim

White, M., C. Mohn, H.C. De Stigter, G. Mottram. 2005. Deep-water coral development as a function of hydrodynamics and surface productivity around the submarine banks of the Rockall Trough, NE Atlantic. In A. Freiwald and J. M. Roberts (eds), Cold-water corals and ecosystems. Springer-Verlag: 503-514

White, M., G.A. Wolff, T. Lundälv, D. Guihen, K. Kiriakoulakis, M. Lavaleye, G. Duineveld. 2012. Cold-water coral ecosystem (Tisler Reef, Norwegian Shelf) may be a hotspot for carbon cycling. Marine Ecology Progress Series, 465: 11-23, doi:10.3354/meps09888

Youngbluth, M.J., T.G. Bailey, P.J. Davoll, C.A. Jacoby, P.I. Blades-Eckelbarger, C.A. Griswold 1989. Fecal pellet production and diel migratory behavior by the euphausiid *Meganyctiphanes norvegica* effect benthic-pelagic coupling. Deep Sea Research Part A. Oceanographic Research Papers, 36(10), 1491-1501

Zhu, Y., Tande, K.S., Zhou, M., 2009. Mesoscale physical processes and zooplankton productivity in the northern Norwegian shelf region. Deep-Sea Research II, 56: 1922-1933, doi:10.1016/j.dsr2.2008.11.019

Acknowledgments

We gratefully acknowledge Equinor ASA and the Research Council of Norway for funding the

Lofoten-Vesterålen cabled observatory (contract 245843). We also thank Tim Nattkemper, Jonas Osterloff and the reviewers for their valuable input. This research was supported by the European Union's Horizon 2020 research and innovation programme under grant agreement No. 678760 (ATLAS) and the Netherlands Organisation for Scientific Research (NWO-VIDI grant no. 864.13.007).